Cold-Atom Physics Using Ultrathin Optical Fibers: Light-Induced Dipole Forces and Surface Interactions

G. Sagué, E. Vetsch, W. Alt, D. Meschede, and A. Rauschenbeutel*

Institut für Angewandte Physik, Universität Bonn, Wegelerstr. 8, 53115 Bonn, Germany

(Received 22 January 2007; published 16 October 2007)

The strong evanescent field around ultrathin unclad optical fibers bears a high potential for detecting, trapping, and manipulating cold atoms. Introducing such a fiber into a cold-atom cloud, we investigate the interaction of a small number of cold cesium atoms with the guided fiber mode and with the fiber surface. Using high resolution spectroscopy, we observe and analyze light-induced dipole forces, van der Waals interaction, and a significant enhancement of the spontaneous emission rate of the atoms. The latter can be assigned to the modification of the vacuum modes by the fiber.

DOI: 10.1103/PhysRevLett.99.163602 PACS numbers: 34.50.Dy, 32.80.Pj, 39.25.+k, 42.50.−p

Tapered and microstructured optical fibers count among the most active fields of research in recent years [1,2]. In such fibers, the propagation of light can, e.g., be tailored such that it controllably depends on the light intensity. These fiber-induced nonlinear processes play for instance a major role in the generation of optical frequency combs and often stem from the nonlinear response of the bulk fiber material, subjected to extreme intensities. The low intensity limit of nonlinear light-matter interaction is reached when single photons already induce a nonlinear response of matter. This situation is realized in cavity quantum electrodynamics [3], where photons, typically confined in space by an optical resonator [4], interact with a single or a few dipole emitters.

In this context, ultrathin unclad optical fibers offer a strong transverse confinement of the guided fiber mode while exhibiting a pronounced evanescent field surrounding the fiber [5]. This unique combination allows to efficiently couple particles (atoms, molecules, quantum dots, etc.) on or near the fiber surface to the guided fiber mode, making tapered optical fibers (TOFs) a powerful tool for their detection, investigation, and manipulation: The absorbance of organic dye molecules, deposited on a subwavelength-diameter TOF, has been spectroscopically characterized via the fiber transmission with unprecedented sensitivity [6]. Furthermore, the fluorescence from a very small number of resonantly irradiated atoms around a 400-nm diameter TOF, coupled into the guided fiber mode, has been detected and spectrally analyzed [7,8]. Finally, it has also been proposed to trap atoms around ultrathin fibers using the optical dipole force exerted by the evanescent field [9,10].

Here, we report on the observation of such dipole forces induced by the evanescent field around a subwavelength diameter TOF. By spectroscopically investigating the transmission of a probe laser launched through the fiber, we find clear evidence of the mechanical effects of these dipole forces on the atoms, leading to a modification of the atomic density in the vicinity of the fiber. A rigorous analysis furthermore shows that a detailed description of the absorption signal must include the interaction of the atoms with the dielectric fiber. In particular, this includes the mechanical and spectral effects of the van der Waals (vdW) interaction and a significant enhancement of the spontaneous emission rate of the atoms due to a modification of the vacuum modes by the fiber. A modified spontaneous emission *in vacuo* close to a dielectric was so far only observed with atoms near a plane interface [11]. Here, the atoms are interacting with a cylindrical ultrathin dielectric fiber which, in difference to the plane geometry above, also sustains a strongly confined guided mode. This mode significantly contributes to the enhancement of the spontaneous emission [7], an effect which, to our knowledge, has never been observed before without a cavity.

Figure 1(a) shows the schematic experimental setup. A cloud of cold cesium atoms, released from a magneto-optical trap (MOT), is spatially overlapped with the waist of a TOF in an ultra high vacuum (UHV) environment. The MOT is geometrically aligned by means of a bias magnetic field while monitoring its position with two CCD cameras. A frequency scanned probe laser is launched through the

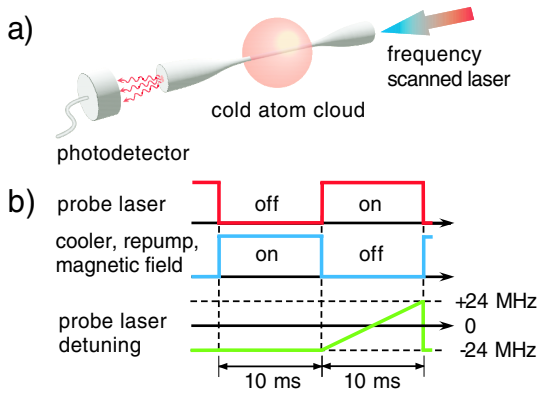

FIG. 1 (color online). (a) Schematic experimental setup. A cloud of laser cooled cesium atoms is spatially overlapped with the 500-nm diameter waist of a tapered optical fiber. The transmission through the fiber is measured using a photodetector. (b) Timing of the experiment.

fiber and its transmission is measured with an avalanche photodiode (APD). Typical powers of the probe laser used in the experiment range from several hundred femtowatts to one nanowatt.

We fabricate the tapered fibers by stretching a standard single mode fiber (Newport F-SF) while heating it with a traveling hydrogen/oxygen flame [12]. Our computer controlled fiber pulling rig produces tapered fibers with a homogeneous waist diameter down to 100 nm and a typical extension of 1–10 mm. For TOFs with final diameter above 0.5 μm, we achieve up to 97% of the initial transmission at 852 nm. For the present experiment we used a 500-nm diameter fiber with 93% transmission and a waist length of 5 mm, sustaining only the fundamental mode at the 852-nm Cs $D2$ wavelength. During evacuation of the vacuum chamber, the fiber transmission dropped to 40%, possibly due to contamination with pump oil. After 1 d in UHV, the transmission increased again to 80%.

We use a conventional Cs MOT with a $1/\sqrt{e}$-radius of 0.6 mm. We probe the atoms with a diode laser which is frequency scanned by ± 24 MHz with respect to the $6\,^2S_{1/2}$, $F = 4$ to $6\,^2P_{3/2}$, $F = 5$ transition using an acousto-optical modulator in double pass configuration. While being linearly polarized before coupling into the TOF, the probe laser polarization at the position of the fiber waist is unknown. The probe laser linewidth of 1 MHz allows to resolve the 5.2-MHz natural linewidth of the Cs $D2$ line in Doppler-free spectroscopy.

Figure 1(b) shows the timing of the experimental sequence: During the first 10 ms, the atoms are captured and cooled in the MOT while the probe laser is off. In the following 10 ms, the MOT cooling- and repump-laser and the magnetic field are off and the probe laser is on. The atoms are thus not influenced by the MOT beams or magnetic fields during the spectroscopy.

The APD signal is recorded with a digital storage oscilloscope and averaged over 4096 traces. Figure 2 shows the measured (line graphs) and theoretically predicted (squares) absorbance of the atoms (negative natural logarithm of the transmission) versus the probe laser detuning for three different probe laser powers. The theory assumes an averaged atomic density distribution $\rho_{\delta,P}(r, z)$ around the fiber, where r is the distance from the fiber center and z the position along the fiber waist. Note that, due to light-induced dipole forces, $\rho_{\delta,P}$ also depends on the detuning of the probe laser with respect to resonance, δ, and on its power, P. The line shape is then given by

$$A_P(\delta) = \frac{\hbar w}{P} \int \rho_{\delta,P}(r, z)\Gamma(I_P(r), \gamma(r), \delta + \delta_{\mathrm{vdW}}(r))dV, \tag{1}$$

where $\Gamma(I_P(r), \gamma(r), \delta + \delta_{\mathrm{vdW}}(r))$ is the scattering rate of an atom in the evanescent field with intensity $I_P(r)$, $\gamma(r)$ is the longitudinal decay rate of the atom, and $\delta_{\mathrm{vdW}}(r)$ is the vdW shift of the atomic transition frequency.

The evanescent field intensity profile, $I_P(r)$, can be found in [5]. The polarization state of the evanescent field has been assumed to be an incoherent, equally weighted mixture of linearly and circularly polarized light. Under these conditions, the Cs saturation intensity in free space is 18 W/m^2. The longitudinal decay rate strongly depends on the atom-fiber distance [13]. Given that the silica fiber is transparent at the Cs $D2$ wavelength, $\gamma(r)$ has only two contributions: emission into freely propagating modes and emission into guided fiber modes

$$\gamma(r) = \gamma_{\mathrm{free}}(r) + \gamma_{\mathrm{guid}}(r). \tag{2}$$

For an atom near a 500-nm diameter dielectric cylinder at distances smaller than the emission wavelength, $\gamma_{\mathrm{free}}(r)$ is given in [13] while $\gamma_{\mathrm{guid}}(r)$ can be approximated as

$$\gamma_{\mathrm{guid}}(r) \simeq 0.3\gamma_0 I_P(r)/I_P(a). \tag{3}$$

Here, γ_0 is the spontaneous emission rate of a Cs atom in free space, a denotes the fiber radius, and $0.3\gamma_0$ corresponds to the spontaneous emission rate of an atom placed on the surface of a 500 nm diameter optical fiber into the guided mode [7]. On the surface of the fiber, Eq. (2) then predicts a 57% increase of the spontaneous emission rate of the Cs atoms, resulting in a broadening of the absorbance line shapes.

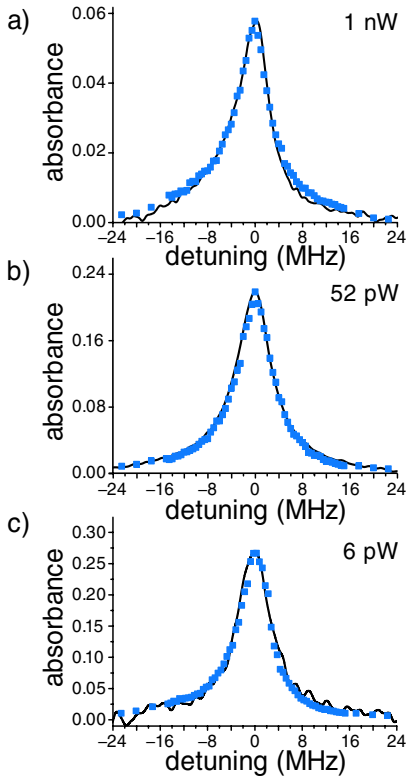

FIG. 2 (color online). Measured (line graphs) and simulated (squares) absorbance of the atoms versus the detuning of the probe laser. The effective number of atoms contributing to the spectra [see Eq. (5)] is 107, 14, and 2 for (a) 1 nW, (b) 52 pW, and (c) 6 pW of probe laser power, respectively. The decrease of the peak absorbance with increasing power is due to the saturation of the atoms.

We calculated the vdW shift, $\delta_{\mathrm{vdW}}(r)$, for the $D2$ line of Cs near a 500 nm diameter dielectric cylinder [14]. It stems from the different polarizabilities of the $6\,^2S_{1/2}$ ground state and the excited $6\,^2P_{3/2}$ state of the Cs atoms when interacting with the dielectric surface. According to Eq. (1), $\delta_{\mathrm{vdW}}(r)$ thus inhomogeneously broadens the absorbance profile: Atoms at different distances from the fiber surface will be unequally shifted while contributing to $A_P(\delta)$. Furthermore, we expect the center of the profile to be red-shifted by at most -0.5 MHz. However, being of the same order as the drifts of our probe laser frequency, this shift is too small to be experimentally quantified using the current setup.

Finally, we assume the following explicit form for the density distribution of the atomic cloud:

$$\rho_{\delta,P}(r,z) = \left\{\frac{n_0}{\sigma^3(2\pi)^{3/2}}\, e^{-((r^2+z^2)/(2\sigma^2))}\right\} f_{\delta,P}(r). \qquad (4)$$

Here, the term in curly brackets corresponds to a Gaussian density distribution of the unperturbed atomic cloud with $\sigma = 0.6$ mm radius, containing n_0 atoms. The factor $f_{\delta,P}(r)$ accounts for the perturbation introduced by the presence of the fiber. We calculate $f_{\delta,P}(r)$ with a Monte Carlo simulation of 100 000 trajectories of thermal atoms with a temperature of 125 μK, i.e., the Cs Doppler temperature. This simulation includes the attractive vdW force between the fiber surface and the atoms and the saturating dipole force induced by the probe laser [15].

Figure 3(a) shows $f_{\delta,P}(r)$ as a function of the distance from the fiber surface for $P = 1$ nW and $\delta = -3$, 0, and $+3$ MHz (dotted, solid, and dashed line). The frequency dependency of $f_{\delta,P}(r)$ due to light-induced dipole forces is clearly apparent. In all three cases $f_{\delta,P}(r)$ decays to zero at the surface of the fiber due to the vdW force.

$A_P(\delta)$ from Eq. (1) can now be adjusted to the experimental line shapes, the only fitting parameters being n_0 and an experimental frequency offset. Figure 2 shows three examples for P ranging over 3 orders of magnitude. The agreement between theory (squares) and experiment (line graphs) is excellent. In particular, in addition to the line width, our model reproduces well the asymmetry of the line shape observed for larger powers.

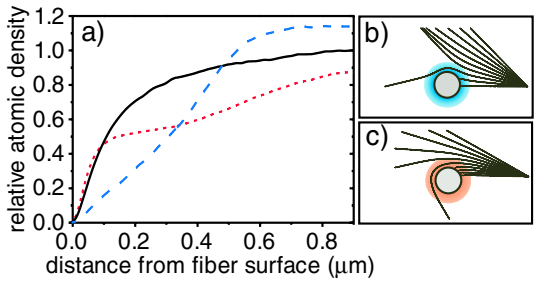

FIG. 3 (color online). (a) Simulations of the relative density of the MOT for different detunings δ of the probe laser versus the distance from the fiber surface; solid line $\delta = 0$ MHz, dotted line $\delta = -3$ MHz, dashed line $\delta = 3$ MHz. The following parameters have been used for the simulations: Fiber diameter 500 nm, probe power 1 nW and a 3D Maxwellian velocity distribution of the Cs atoms at a temperature of 125 μK. (b) and (c) show several atomic trajectories for $\delta = +3$ MHz and $\delta = -3$ MHz, respectively, with a fixed atom velocity of 10 cm/s.

Figure 4 shows the width of the measured absorbance profiles versus the probe laser power (squares). The linewidths predicted by our model are also shown (open circles with a b-spline fit as a guide to the eye). We recall that the effects of light-induced dipole forces and surface interactions have been included in the model. For comparison, we also show the expected linewidths in absence of these effects (dashed line). While the full model agrees very well with the experimental data, the reduced model strongly deviates both for high and low powers.

For probe laser powers larger than 100 pW, the measured lines are considerably narrower than what would be expected in absence of dipole forces and surface interactions; see Fig. 4(a). For 1 nW of probe laser power this narrowing exceeds 40%. The narrowing can be explained by the effect of the light-induced dipole forces on the density of the atomic cloud; see Fig. 3(a). For distances smaller than 370 nm, i.e., in the region that contains more than 75% of the evanescent field power, the largest integrated density of the atomic cloud is predicted in the case of zero detuning ($\delta = 0$ MHz). For blue ($\delta = +3$ MHz) and red ($\delta = -3$ MHz) detunings, this integrated density is lowered due to the effect of the light-induced dipole forces. This results in a reduced absorbance and leads to an effective line narrowing. Figures 3(b) and 3(c) show several simulated atomic trajectories with fixed initial velocity. For the case of blue detuning, (b), the atoms are repelled by the fiber due to the repulsive light-induced dipole force. For the case of red detuning, (c), the atoms are accelerated towards the fiber. Naively, one might assume that this increases the density close to the fiber. However, this effect is counteracted by the shorter average time of flight of the atoms through the evanescent field due to their higher velocity and by the higher atomic loss rate [16]. In fact, for distances up to 100 nm both effects cancel almost perfectly. For larger distances, however, the effects reducing the density dominate. The net effect is therefore also a reduction of the absorbance.

Figure 4(b) shows the linewidths for the limit of low probe laser powers, i.e., low saturation and negligible light-induced dipole forces. The measured linewidths approach 6.2 MHz for vanishing powers. This result exceeds the natural Cs $D2$ linewidth in free space by almost 20%. This broadening can be explained by surface interactions, i.e., the vdW shift of the Cs $D2$ line and the modification of the spontaneous emission rate of the atoms near the fiber, see Eq. (1). Both effects have the same magnitude and only their combination yields the very good agreement between our model and the experimental data.

Finally, we estimate the effective number, N_P, of fully saturated atoms contributing to the signals in Fig. 2. From

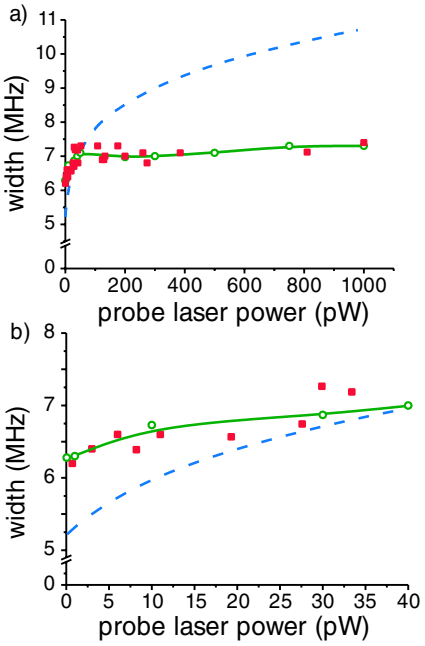

FIG. 4 (color online). Linewidth of the absorbance profiles versus probe laser power. (a) full power range and (b) low power range. The squares correspond to the experimental data and the open circles are the simulated values. The continuous line is a guide to the eye (b-spline) of the simulated values. The dashed line is the reduced model not taking into account light-induced dipole forces and surface interactions.

the adjustment of the height of the absorbance profiles, we extract the total number of atoms in the cloud, n_0, and infer a maximum atomic density of 4.4×10^{10} atoms/cm^3 using Eq. (4). This value is slightly smaller than typical peak densities of unperturbed Cs MOTs [17]. We now estimate N_P according to

$$N_P = \frac{2}{\gamma_0} \int \rho_{\delta=0,P}(r, z)\Gamma(I_P(r), \gamma(r), \delta_{\mathrm{vdW}}(r))dV, \quad (5)$$

where we follow the notation of Eq. (1). Note that N_P is power dependent and can be lowered by reducing P. We calculate N_P to be 107, 14, and 2 in Figs. 2(a)–2(c), respectively. Furthermore, due to the saturating scattering rate Γ in the integrand of Eq. (5), the mean distance of the probed atoms from the fiber surface is also power dependent and can be adjusted down to 248 nm.

Summarizing, we have shown that subwavelength diameter optical fibers can be used to detect, spectroscopically investigate, and mechanically manipulate extremely small samples of cold atoms. In particular, on resonance, as little as two atoms on average, coupled to the evanescent field surrounding the fiber, already absorbed 20% of the total power transmitted through the fiber. These results open the route towards the use of ultrathin fibers as a powerful tool in quantum optics and cold-atom physics. By optically trapping one or more atoms around such fibers [9,10], it should become possible to deterministically couple the atoms to the guided fiber mode and to even mediate a coupling between two simultaneously trapped atoms [18], leading to a number of applications, e.g., in the context of quantum information processing. In addition, high precision measurements of the modification of the lifetime of atomic energy levels near surfaces and of the van der Waals potential [19] are also within the scope of such glass fiber quantum optics experiments.

We wish to thank V. I. Balykin and D. Haubrich for their contribution in the early stages of the experiment, F. Warken for assistance in the fiber production, B. Weise for his part in the simulations, and M. Ducloy and C. Henkel for valuable discussions. This work was supported by the EC (Research Training Network "FASTNet") and the DFG (Research Unit 557).

*Present address: Institut für Physik, Universität Mainz, 55099 Mainz, Germany.
rauschenbeutel@uni-mainz.de

[1] P. Russell, Science **299**, 358 (2003).
[2] L. Tong *et al.*, Nature (London) **426**, 816 (2003).
[3] *Cavity Quantum Electrodynamics*, edited by P. R. Berman (Academic, New York, 1994).
[4] K. J. Vahala, Nature (London) **424**, 839 (2003).
[5] F. Le Kien, J. Q. Liang, K. Hakuta, and V. I. Balykin, Opt. Commun. **242**, 445 (2004).
[6] F. Warken, E. Vetsch, D. Meschede, M. Sokolowski, and A. Rauschenbeutel, arXiv:cond-mat/0701264.
[7] Fam Le Kien, S. Dutta Gupta, V. I. Balykin, and K. Hakuta, Phys. Rev. A **72**, 032509 (2005).
[8] K. P. Nayak *et al.*, arXiv:quant-ph/0610136.
[9] J. P. Dowling and J. Gea-Banacloche, Adv. At. Mol. Opt. Phys. **37**, 1 (1996).
[10] Fam Le Kien, V. I. Balykin, and K. Hakuta, Phys. Rev. A **70**, 063403 (2004).
[11] V. V. Ivanov, R. A. Cornelussen, H. B. van Linden van den Heuvell, and R. J. C. Spreeuw, J. Opt. B **6**, 454 (2004).
[12] T. A. Birks and Y. W. Li, J. Lightwave Technol. **10**, 432 (1992).
[13] V. V. Klimov and M. Ducloy, Phys. Rev. A **69**, 013812 (2004).
[14] M. Boustimi, J. Baudon, P. Candori, and J. Robert, Phys. Rev. B **65**, 155402 (2002).
[15] J. E. Bjorkholm, R. R. Freeman, A. Ashkin, and D. B. Pearson, Phys. Rev. Lett. **41**, 1361 (1978).
[16] Upon collision with the fiber surface, the atoms are either adsorbed or rapidly expelled with a kinetic energy of $E_{\mathrm{kin}}/k_B \approx 300$ K and do not contribute to the absorbance signal anymore.
[17] C. G. Townsend *et al.*, Phys. Rev. A **52**, 1423 (1995).
[18] Fam Le Kien, S. Dutta Gupta, K. P. Nayak, and K. Hakuta, Phys. Rev. A **72**, 063815 (2005).
[19] M. Chevrollier, D. Bloch, G. Rahmat, and M. Ducloy, Opt. Lett. **16**, 1879 (1991).